PHYSICAL REVIEW B **88**, 134404 (2013)

Evolution of incommensurate spin order with magnetic field and temperature in the itinerant antiferromagnet GdSi

Yejun Feng,[1,2] D. M. Silevitch,[2] Jiyang Wang,[2] A. Palmer,[2] Nayoon Woo,[2] J.-Q. Yan,[3,4] Z. Islam,[1] A. V. Suslov,[5]
P. B. Littlewood,[2,6] and T. F. Rosenbaum[2]
[1]*The Advanced Photon Source, Argonne National Laboratory, Argonne, Illinois 60439, USA*
[2]*The James Franck Institute and Department of Physics, The University of Chicago, Chicago, Illinois 60637, USA*
[3]*Department of Materials Science and Engineering, University of Tennessee, Knoxville, Tennessee 37996, USA*
[4]*Materials Science and Technology Division, Oak Ridge National Laboratory, Oak Ridge, Tennessee 37831, USA*
[5]*National High Magnetic Field Laboratory, Tallahassee, Florida 32310, USA*
[6]*Physical Sciences and Engineering, Argonne National Laboratory, Argonne, Illinois 60439, USA*
(Received 17 July 2013; published 7 October 2013)

GdSi exhibits spin-density-wave (SDW) order arising from the cooperative interplay of sizeable local moments and a partially nested Fermi sea of itinerant electrons. Using magnetotransport, magnetization, and nonresonant magnetic x-ray diffraction techniques, we determine the *H*-*T* phase diagrams of GdSi for magnetic fields up to 21 T, where antiferromagnetic order is no longer stable, and field directions along each of the three major crystal axes. While the incommensurate magnetic ordering vector that characterizes the SDW is robust under magnetic field, the multiple spin structures of this compound are highly flexible and rotate relative to the applied field via either canting or spin-flop processes. The antiferromagnetic spin densities always arrange themselves transverse to the applied magnetic field direction. The phase diagrams are delineated by two types of phase boundaries: one separates a collinear from a planar spin structure associated with a lattice structural transition, and the other defines a spin flop transition that is only weakly temperature dependent. The major features of the phase diagrams along each of the crystal axes can be explained by the combination of local moment and global Fermi surface physics at play.

DOI: 10.1103/PhysRevB.88.134404 PACS number(s): 75.30.Fv, 75.30.Kz, 75.25.−j, 72.15.Gd

I. INTRODUCTION

There are two typical mechanisms for creating incommensurate spin ordering in metals. In one limit, an incommensurate structure can arise from purely itinerant spins. The archetypical example is the spin density wave (SDW) in Cr,[1] which is driven by nesting of the Fermi surface.[2] In the opposite limit, an incommensurate spin structure can be formed from local magnetic moments mediated by itinerant electrons through the Ruderman-Kittel-Kasuya-Yosida (RKKY) exchange interaction. Prominent examples include $\mathrm{PrNi_2Si_2}$ (Ref. 3), $R\mathrm{Ni_2Ge_2}$ ($R =$ Pr, Nd, Sm, Gd-Tm),[4] $R\mathrm{Co_2Ge_2}$ ($R =$ Gd, Tb, Dy, Ho),[5] and $R\mathrm{Ni_2B_2C}$ ($R =$ Gd, Tb, Ho, Er, and Tm),[6] where all the lanthanide $4f$ moments are well localized. These systems share a $\mathrm{ThCr_2Si_2}$-type tetragonal space group ($I4/mmm$)[7] and are similarly structured with individual R or RC layers separated by T_2X_2 ($T =$ Co, Ni, Cu; $X =$ B, Si, Ge) layers. Although incommensurate magnetic structures are often observed below the Néel temperature,[3–7] there is no resistivity anomaly at the magnetic transition in $\mathrm{PrNi_2Si_2}$ (Ref. 3), $R\mathrm{Ni_2Ge_2}$ ($R =$ La-Nd, Sm-Yb),[8] or $R\mathrm{Ni_2B_2C}$ ($R =$ Gd, Tb, Er).[9] The incommensurate wave vector does not intersect the paramagnetic (PM) Fermi surface, and there is no band gap opened upon magnetic ordering, distinguishing these magnetic transitions from those dependent upon a nesting condition.

In systems with both itinerant and local moments, Fermi surface nesting and the RKKY mechanism are not necessarily mutually exclusive. Recently, a cooperative scenario involving these two effects was identified as the source of the incommensurate SDW in GdSi.[10] The rise of incommensurate antiferromagnetic order in GdSi is accompanied by significant Fermi surface gapping, and the nesting condition for itinerant spins sets a strict constraint on the magnetic wave vector. This is in contrast to the broad maximum in $J(q)$ seen for local moments coupled via the RKKY interaction. The combination of the nested itinerant electrons and the local moments forms a self-consistent whole, with the itinerant electrons mediating the RKKY exchange interaction between the local moments and the ordered local moments providing coupling strength for paired itinerant electrons through a scattering process.[10] This new mechanism for SDW formation provides sufficient freedom for multiple antiferromagnetic phases. We explore here the relationship between the phases, delineate their spin structures, and follow their complete evolution with temperature and magnetic field.

The crystal structure of GdSi in the PM phase[11] is of the orthorhombic space group ($Pnma$, #63), as illustrated in Fig. 1(a). An antiferromagnetic phase transition previously observed at $T = 55$ K (Refs. 12 and 13) was recently resolved to be an antiferromagnetic transition with Néel temperature $T_N = 54.4$ K, followed by a spin-flip transition at $T_{\mathrm{SF}} = 53.0$ K (Ref. 10). X-ray magnetic diffraction revealed details of the spin order with an incommensurate wave vector $\boldsymbol{Q} = (0, q_b, q_c) \sim (0, 0.483, 0.092)$ at $T = 4$ K [Fig. 1(b)]. Collinear spin order first develops upon cooling between T_N and T_{SF}, with all spins aligned transverse to the $\boldsymbol{Q}$ wave vector and within the ***bc*** plane[10] (Fig. 2). Below T_{SF}, this collinear spin structure is transformed by a spin-flip process into a planar spin ordering, which remains transverse to the wave vector $\boldsymbol{Q}$ (Ref. 10; Fig. 3). Below T_{SF}, the crystal lattice also experiences a symmetry reduction into a monoclinic structure (space group

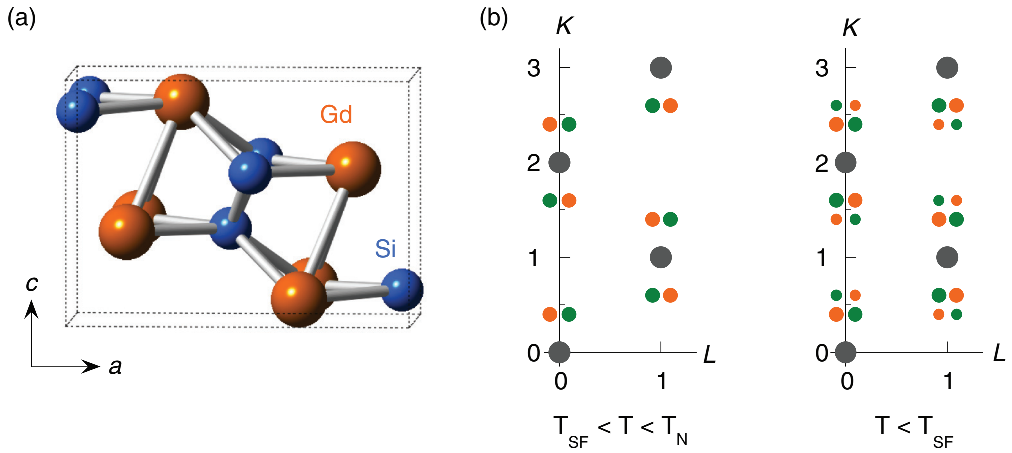

FIG. 1. (Color online) (a) Orthorhombic lattice structure of GdSi, with four chemical units inside one unit cell. (b) Lattice (gray) and magnetic (orange and green) diffraction patterns of GdSi in the KL plane. In the collinear phase between the Néel temperature T_N and the spin-flip temperature T_{SF}, the magnetic peaks are found surrounding all nonforbidden lattice peaks such as (0, 2, 0) and (0, 1, 1) with a spin-ordering wave vector $\boldsymbol{Q} = (0, q_b, q_c) \sim (0, 0.483, 0.093)$. Below T_{SF}, magnetic diffraction is also observed surrounding forbidden lattice orders such as (010), with much lower intensities. There are two degenerate magnetic domains with $\boldsymbol{Q} = (0, \pm q_b, q_c)$ (orange and green) between T_N and T_{SF}. The magnetic structure is a single-q type that is similar to the SDW state in Cr (Refs. [1], [25], and [26]) but different from the double-q state in $\mathrm{HoNi_2B_2C}$ (Ref. [28]) and $\mathrm{GdNi_2B_2C}$ (Ref. [31]). Below T_{SF}, the orthorhombic lattice structure transforms into monoclinic and the magnetic degeneracy is lifted as each magnetic domain becomes associated with the lattice structure.

$P2_1/c$, #14) with the monoclinic angle $\alpha = 89.916°$ between the b and c axes at $T = 4$ K.[10]

Previous work on GdSi[12–14] has shown that the antiferromagnetic order is robust up to approximately 20 Tesla at cryogenic temperatures. However, the H-T phase diagram is not complete,[12–15] and a detailed understanding of the spin structure is missing. Through a combination of the resistivity $\rho(T, H)$, magnetization $M(T, H)$, and synchrotron x-ray diffraction, we map out the full phase diagram and spin structures for magnetic fields applied along all three crystal axes. We pictorially summarize our results for the collinear and planar spin regimes in Figs. 2 and 3, respectively, with the measured phase boundaries plotted in Fig. 4. For $H \| b$ (Fig. 4, top), the in-field behavior in both regimes consists of a continuous canting of the spins towards the field axis. For $H \| a$ (Fig. 4, middle), an additional first-order spin-flop transition is observed in the planar regime. For $H \| \boldsymbol{c}$ (Fig. 4, bottom), this spin-flop transition line extends to span both the planar and collinear regimes. Hence, the overall phase diagram can be described as consisting of two essentially independent phase boundary lines. The first marks the transition between

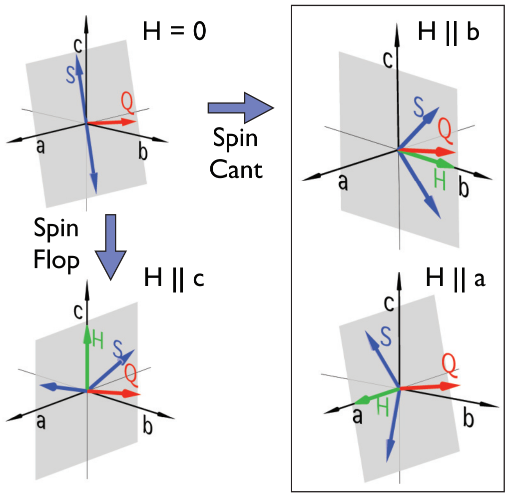

FIG. 2. (Color online) Collinear spin structure in magnetic field. Between T_{SF} and T_N, spins in GdSi are transverse to the magnetic wave vector $\boldsymbol{Q}$ and at $H = 0$ lie within the bc plane. When H is applied along either a or b, the spins continuously cant towards H. For $H \| c$, spins initially experience a first order spin-flop transition before canting further toward H.

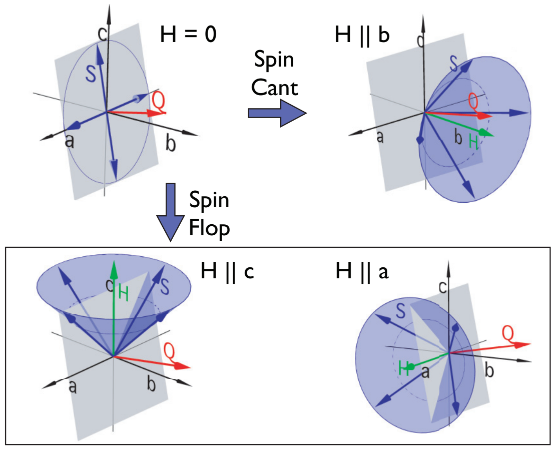

FIG. 3. (Color online) Planar spin structure in a magnetic field. Below T_{SF}, the planar spin structure is transverse to the magnetic wave vector $\boldsymbol{Q}$ at zero field. For $H \| b$, all spins continuously cant towards H. For both $H \| a$ and $H \| c$, about half of the spins experience a spin-flop transition. Eventually the spin component along H is totally ferromagnetic, while the spin component transverse to H is antiferromagnetic.

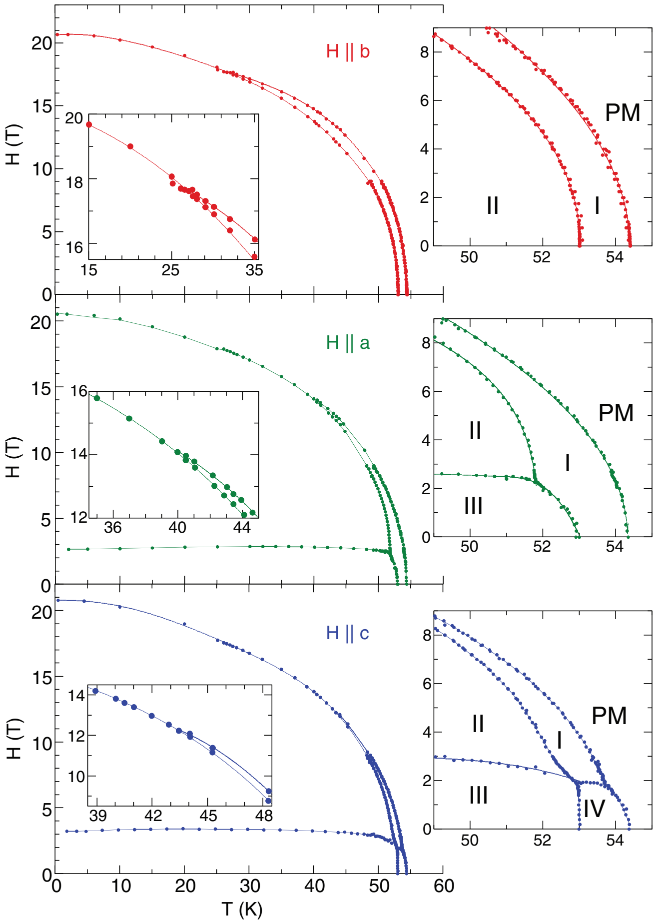

FIG. 4. (Color online) Phase diagrams of GdSi with H parallel to b, a, and c (top to bottom). The insets show detailed regions around the high-field triple point between the collinear, planar antiferromagnetic, and PM phases. The four antiferromagnetic (I to IV) and paramagnetic (PM) phases are marked in blowup views of regions at low field and high temperature for each field configuration.

the collinear and planar regimes and largely parallels the PM boundary until merging with it at magnetic fields between 10 and 20 T depending upon crystal direction. The second phase line denotes the spin-flop transition and has H of order 2 to 4 Tesla at all temperatures, only slowly varying for a given axis.

II. EXPERIMENTAL METHODS

GdSi single crystals approximately 4 mm in diameter and 70 mm in length were grown under a purified Ar atmosphere by the floating zone technique.[13] Room temperature x-ray powder diffraction on pulverized single crystals confirmed that the crystals are single phase. Elemental analysis using a Hitachi TM-3000 tabletop electron microscope equipped with a Bruker Quantax70 energy dispersive x-ray system confirmed the stoichiometric Gd:Si ratio. X-ray Laue imaging was employed to orient the crystals with an accuracy of 1°. Crystals were cut to size using either an acid saw or electrical discharge machining. All samples surfaces were polished to a mirror finish with 0.05-μm alumina suspensions (Buehler).

Magnetization (dc susceptibility) measurements for $0 < H < 5$ T along all three crystal axes were carried out using a Quantum Design MPMS superconducting quantum interference device (SQUID) magnetometer. Magnetoresistance measurements were performed in a four-probe geometry on bar-shaped samples, using an ac resistance bridge (Linear Research LR700 or Lakeshore LS370 with a 3708 preamplifier) in a Quantum Design PPMS up to $H = 9$ T. Additional $\rho(H, T)$ measurements at high magnetic fields were performed at the National High Magnetic Field Laboratory in Tallahassee, using either a 35 T resistive magnet or an 18 T superconducting magnet, both equipped with a Helium-3 sample cryostat. All measurements were performed with the magnetic field aligned along one of the three major crystalline axes. Resistivity values reported here have a systematic error of ±5% due to uncertainties in dimensions.

In-field x-ray magnetic diffraction measurements were performed at beamline 6-ID-B of the Advanced Photon Source using 20 keV x rays. A cryogen-free superconducting magnet provided magnetic fields up to 4.2 T in the vertical direction, perpendicular to the horizontal scattering plane. The x rays were linearly polarized in the horizontal plane at the synchrotron radiation source, and for our nonresonant x-ray magnetic diffraction, this is denoted as π polarization, in contrast to the σ polarization out of the diffraction plane.[16] We used a NaI scintillation detector without any polarization analyzer, summing over both σ and π-polarized diffracted x rays. Individual single crystals of GdSi oriented to have $H\|a$ and $H\|c$ were studied in the transmission and reflection geometries, respectively; the transmission mode sample was thinned to 40 μm. Samples were attached to copper mounts by either silver epoxy (Bacon Industries) or GE7031 varnish and cooled by a variable temperature insert in vacuum inside the superconducting magnet's bore. The limited opening angle of the magnet in the vertical direction confined the accessible diffraction orders to lie close to the (0, K, L) or (H, K, 0) planes for $H\|a$ and $H\|c$, respectively. For the $H\|a$ geometry, we tracked both the (0, 2, 0) and (0, 4, 2) lattice orders, and the $(0, 2 - q_b, -q_c)$ and $(0, 2 + q_b, q_c)$ magnetic orders as a function of field at $T = 46$ K. For the $H\|\boldsymbol{c}$ geometry, we studied the $(0, 2 - q_b, -q_c)$ and $(0, 2 + q_b, q_c)$ magnetic orders as a function of field at $T = 4.5$ K and as a function of temperature for $H = 3.8$ T.

III. RESULTS: *H-T* PHASE DIAGRAMS AND SPIN STRUCTURES

The magnetic phase diagrams in Fig. 4 were determined from magnetotransport and magnetization measurements; representative curves are shown in Figs. 5 and 6. Overall, there are four generic types of antiferromagnetic phases. For phases I and IV and the PM phase, the magnetoresistivity $\rho(H) - \rho(0)$ is always negative, while for phases II and III, the magnetoresistivity is often positive (Fig. 5). All phases have nearly quadratic field dependence in the high temperature region with different positive or negative coefficients, and the phase boundaries are located by tracking local extrema in $d\rho/dH$ and $d\rho/dT$. The sign changes of the magnetoresistivity in different phases are presumably a consequence of different scattering processes in the different phases and will be discussed in detail in a subsequent paper. This paper focuses on explication of the phase diagram for which transport provides a signature.

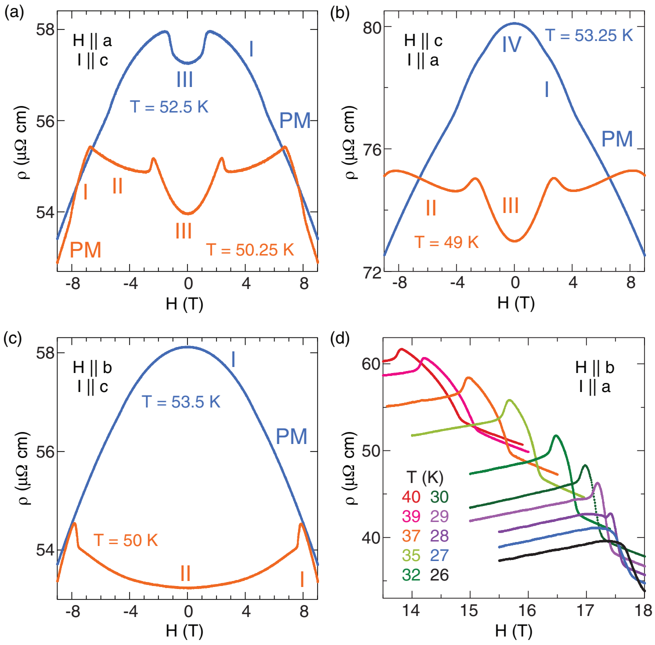

FIG. 5. (Color online) Magnetic field dependence of transverse magnetoresistivity under various field-current configurations of (a) $H\|a$ and $I\|c$; (b) $H\|c$ and $I\|a$; and (c) $H\|b$ and $I\|c$. (d) A set of magnetoresistivity curves with $H\|b$ and $I\|a$ at various temperatures across the triple point at $\sim(H=17.6$ T, $T=27$ K). At high temperature, two well-separated transitions are clearly seen. The transition fields converge with lowering temperature, and eventually become one below $T=28$ K.

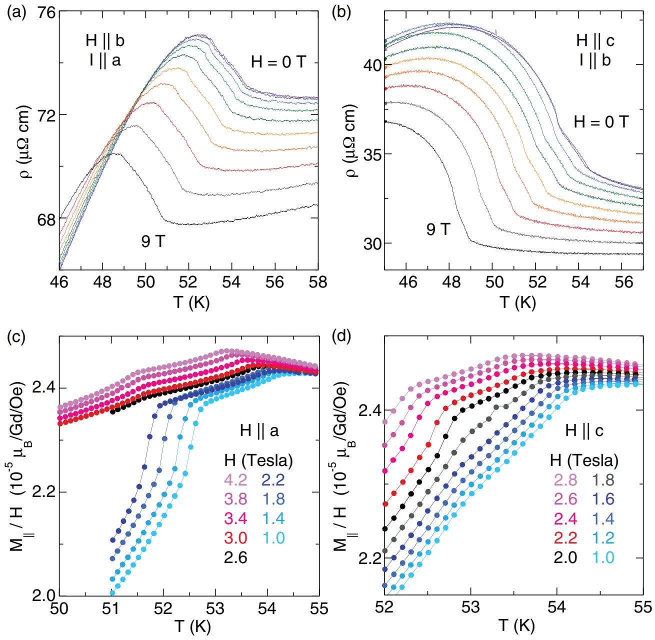

FIG. 6. (Color online) Resistivity of GdSi as a function of temperature measured at 1 T magnetic field intervals from 0 to 9 T for (a) $H\|b$ and $I\|a$ and (b) $H\|c$ and $I\|b$. Susceptibility $M(T)/H$ of GdSi as a function of temperature at various fields for (c) $H\|a$ and (d) $H\|c$.

The phase behavior is simplest for $H\|b$. There are only two antiferromagnetic phases (I and II), and the two phase lines run nearly parallel in H-T space until the triple point with the PM phase is reached at approximately $T=27$ K and $H=17.6$ T (Fig. 4, top). The convergence to the triple point is clearly seen in the set of magnetoresistivity curves in Fig. 5(d). For $H\|a$ and $H\|c$, there are three and four generically different antiferromagnetic phases, respectively (Fig. 4 middle and bottom). The equivalency of individual phases across various phase diagrams becomes clear in light of the dc magnetic susceptibility results and the detailed understanding of the spin structures revealed by x rays, which we discuss below. Here we index various phases by the spin susceptibility, determined by both $M(H)$ and $M(T)/H$ measurements. For $H\|a$, as previously reported,[13,17] $M(H)$ at $T=5$ K exhibits a first-order transition at $H=2.6$ T for the planar spin order [Fig. 7(a)]. Examining the temperature dependence of the susceptibility, $M(T)/H$ [Fig. 6(c)] shows a clear separation of behavior above and below $H=2.6$ T for temperatures below T_{SF}; above T_{SF}, no such separation is observed. This suggests that the first-order transition observed at low temperature is only present in the planar regime and does not extend into the collinear regime. By contrast, for $H\|c$, there are four different antiferromagnetic phases. The low-temperature planar spin order also experiences a phase transition under field [Fig. 7(a)], albeit broader than that of $H\|a$. Moreover, the existence of two spin structures in the collinear interval between T_N and T_{SF} is clearly seen in the different functional dependencies of the $M(T)/H$ curves below and above $H=1.8$ T [Fig. 6(d)]. The high field phase exhibits a $M(T)/H$ behavior similar to that seen for phase I in the $H\|a$ phase diagram. As shown in Fig. 7(a) and also in Ref. 13, the magnetization behavior at $T=5$ K for $H>4$ T is similar for all three axes, indicating that the spin configurations converge in this limit.

Since the magnetism in GdSi arises entirely from spins with no orbital moments, the cross section of nonresonant magnetic x-ray diffraction is proportional to $|S\cdot k(1-k\cdot k')|^2+|S\cdot(k\times k')|^2$ under our diffraction conditions.[16] Given that the diffraction 2θ angle is always less than 24° for our magnetic scattering, this cross section is dominated by the second term with a sensitivity to spin density $S(Q)$ projected out of the diffraction plane, parallel to the field direction under our measurement geometry. This spin component S at a finite Q is antiferromagnetic in contrast to the longitudinal magnetization M measured in a SQUID magnetometer [Figs. 6(c), 6(d), and 7(a)], which yields the ferromagnetic component along the field direction.

At $H=0$ and $T<T_{\mathrm{SF}}$, the spin structure is planar and is transverse to the ordering wave vector $\boldsymbol{Q}$.[10] The finite spin components of antiferromagnetic $S(Q)$ along both the a and c axes emerge clearly in the nonzero x-ray magnetic diffraction intensities at $H=0$ [Fig. 7(b)]. In phase III, $S(Q)$ along the $H\|a$ direction grows sharply under increasing field up to $H=2.3$ T, as the x-ray diffraction intensity is proportional to the square of $S(Q)$. However, no antiferromagnetic $S(Q)$ is detected in phase II [Fig. 7(b)]. On the other hand, the susceptibility dM/dH of the ferromagnetic spin component increases by a factor of three when crossing from phase II to phase III at $T=5$ K [Fig. 7(a)].

For $H\|c$, the antiferromagnetic $S(Q)$ grows by a factor of 1.9 along the field direction in phase III [Fig. 7(b)], while the ferromagnetic component M has a susceptibility similar to that of $H\|a$ [Fig. 7(a)]. However, the transition to phase II is

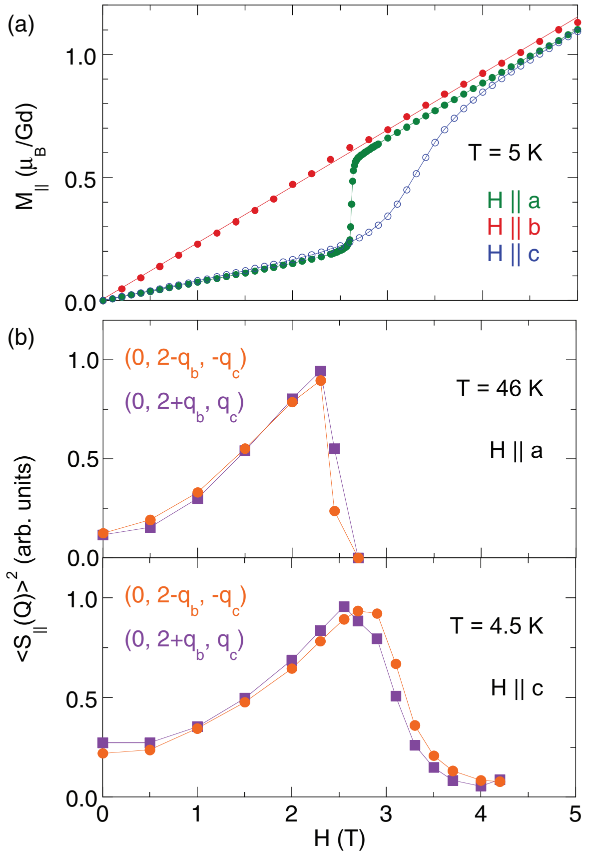

FIG. 7. (Color online) Magnetization versus field in GdSi. (a) The ferromagnetic component of the magnetization along the field direction, measured in a SQUID magnetometer at $T = 5$ K for H along each of the three crystal axes. (b) The antiferromagnetic spin density along the applied field direction, measured by x-ray magnetic diffraction for two magnetic orders $(0, 2 \pm q_b, \pm q_c)$, for $H \| a$ at $T = 46$ K and $H \| c$ at $T = 4.5$ K, respectively.

more gradual, with a broad transition region visible in both the antiferromagnetic $S(Q)$ measurement [Fig. 7(b)] and the ferromagnetic magnetization measurement [Fig. 7(a)]. The $H = 4.2$ T maximum field available for the x-ray measurements does not drive the transition to completion, as evidenced by the small but nonzero $S(Q)$ remaining at that field [Fig. 7(b)]. As noted above, the similar susceptibilities, dM/dH at $H = 5$ T [Fig. 7(a)], indicate that the spin structures in phase II are similar for field along all three axes. The spin component parallel to the magnetic field is solely ferromagnetic, and all antiferromagnetic spin densities are arranged in the plane perpendicular to the field direction. For $H \| b$, the magnetic field direction is nearly parallel to the magnetic ordering vector $\boldsymbol{Q}$, and the spins that are perpendicular to $\boldsymbol{Q}$ at $H = 0$ would gradually cant toward the field direction upon increasing field strength (Figs. 2 and 3). For $H \| a$ and $H \| c$, this is likely also the spin structure in the high field. Starting at low field, the antiferromagnetic spin components aligned along the field direction in phase III would have to experience a spin-flop transition to be transverse to the field in phase II (Fig. 3). Our $M(H)$ curves are consistent with a spin-flop transition similar to what has been observed in many Gd-based antiferromagnets such as Gd_5Ge_4 (Ref. 18), $GdCu_6$ (Ref. 19), and GdB_2C_2 (Ref. 20). For the collinear spin structure between T_N and T_{SF}, a similar argument applies. There is a spin-flop transition in the $H \| c$ geometry but only a continuous spin-canting movement for $H \| a$ and $H \| b$ (Fig. 2).

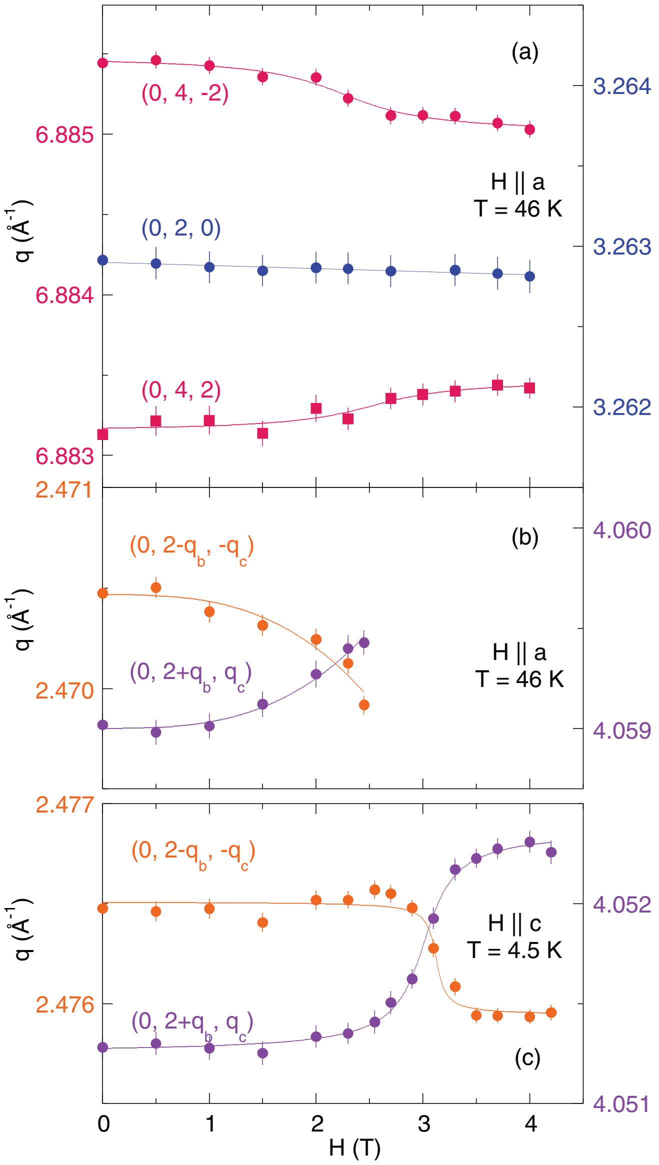

FIG. 8. (Color online) Magnetic field dependence of (a) lattice orders (0, 4, 2) and (0, 2, 0); (b) magnetic vectors $(0, 2 \pm q_b, \pm q_c)$ for $H \| a$ at $T = 46$ K, and (c) magnetic vectors $(0, 2 \pm q_b, \pm q_c)$ for $H \| c$ at $T = 4.5$ K.

Our x-ray diffraction results also specify the lattice symmetry and trace the evolution of the incommensurate spin wave vectors with magnetic field for H up to 4.2 T (Fig. 8). For $H \| a$, a splitting of the $(0, K, L)$ Bragg diffraction peak is clearly seen with the measured (0, 4, 2) order. This reproduces results at $H = 0$, which were attributed to an orthorhombic-monoclinic structural phase transition associated with the collinear-planar spin structure transition.[10] Upon crossing from phase III to II, this monoclinic splitting is slightly reduced but remains finite. Thus we believe that both phases II and III have spin arrangements that are not confined within a single plane (Fig. 3). The b axis lattice constant [measured from the (0, 2, 0) order] remains constant for $H\|a$. Previous magnetostriction measurements also show that the lattice constants a and c stay unchanged under applied field along the axial direction up to the $H\sim 20$ T dissolution of the antiferromagnetism.[14]

With the understanding of the spin behavior illustrated in Figs. 2 and 3, the structure of the phase diagrams as a function of field direction and magnitude becomes clear (Fig 4). There are essentially two phase lines inside the antiferromagnetic phase boundary. One marks the border between the collinear and the planar ordering regimes; this phase line starts at zero field 1.4 K below the PM transition and eventually converges with that boundary, forming a triple point (Fig. 4 insets) The second phase line marks a spin-flop transition as the antiferromagnetic spin density reorients to lie transverse to the applied magnetic field, and this transition line occurs at an essentially constant field. The spin flop transition line terminates in a triple point when intersecting the collinear/planar line ($H\|a$) or the PM transition ($H\|c$). These two phase lines are nearly orthogonal in H-T space and are independent and first order.

The field required to rotate all of the spins into an induced ferromagnetic orientation can be estimated from a single-ion picture as $H_c=\frac{3K_B(T_N-\theta_w)}{gJ\mu_B}$, where the Néel temperature $T_N=54.4$ K, susceptibility measurements in the paramagnet determine the Curie-Weiss temperature θ_W to be -1.6 K,[13] and $J=7/2$. This yields $H_c=36$ T. Experimentally, we measure $H_c=20.7$ T (Fig. 4), with the high field phase boundaries at zero temperature varying in a small range of ± 0.13 T for H along the three crystalline axes ($H_c=20.53$ T for $H\|a$, $H_c=20.66$ T for $H\|b$, and $H_c=20.78$ T for $H\|c$). This indicates a small single-ion anisotropy of $\pm 0.7\%$ for localized Gd $4f$ spins, which is consistent with the observation of isotropic 3D Heisenberg spin fluctuations near the thermal phase boundary at zero field.[10]

Given the absence of any crystal field effects or exchange anisotropy in Gd-based magnets, it has been suggested that the dipolar interaction between Gd moments determines the spin direction in any long-range ordered state.[21] The spin directions have been calculated for magnets with one Gd atom per primitive unit cell and known ordering wave vector by minimizing the dipolar interaction energy, and the theoretical results largely agree with the experimental data.[21] It remains to be seen, however, for a more complicated magnet such as GdSi, with four Gd atoms per FeB-structured orthorhombic unit cell, whether both the collinear and planar spin structures[10] can be predicted by the dipolar interactions. A further complication is that the isotropic exchange constants for all nearest neighbors are required as well to determine the spin-flip transition at $T_{\mathrm{SF}}\sim 0.96\ T_N$ and $H=0$ (Ref. 21) The power of this theoretical construct would be valuable to extend to other FeB-structured Gd-based intermetallic compounds, ranging from the ferromagnets GdPt[22] and Gd($\mathrm{Ni_{0.7}Cu_{0.3}}$)[23] to the helimagnets Gd($\mathrm{Ni_{0.4}Cu_{0.6}}$) with a wave vector $(0,\ 0,\ \frac{1}{4})$[23] and GdCu with a wave vector $(0,\ \frac{1}{4},\ \frac{1}{4})$.[24]

IV. DISCUSSION: INCOMMENSURATE MAGNETIC ORDER IN FIELD

Understanding the spin projections does not directly imply the spin ordering wave vector. We address this issue with in-field x-ray magnetic diffraction. With the slow disappearance of the antiferromagnetic spin density for $H\|c$, we are able to track the magnetic wave vector $\boldsymbol{Q}$ into the high field phase. As shown in Fig. 8, the q values for both the $(0,\ 2-q_b,\ -q_c)$ and the $(0,\ 2+q_b,\ q_c)$ magnetic orders vary only slightly under field for both $H\|a$ and $H\|c$. For $H\|c$, the temperature dependence of $\boldsymbol{Q}(T)$ was also measured at 3.8 T, showing a similar trend to that observed at zero field.[10] Using the relation $q^2_{(0,2\pm q_b,\pm q_c)}=q_c^2+(q_{(020)}\pm q_b)^2$, both incommensurate components of $Q=(0,\ q_b,\ q_c)$ were calculated. The trajectory of Q in the KL plane is also plotted compared to that measured at zero field (Fig. 9), with the assumption that both the b and c lattice constants do not change from their $H=0$ values.[10,14]

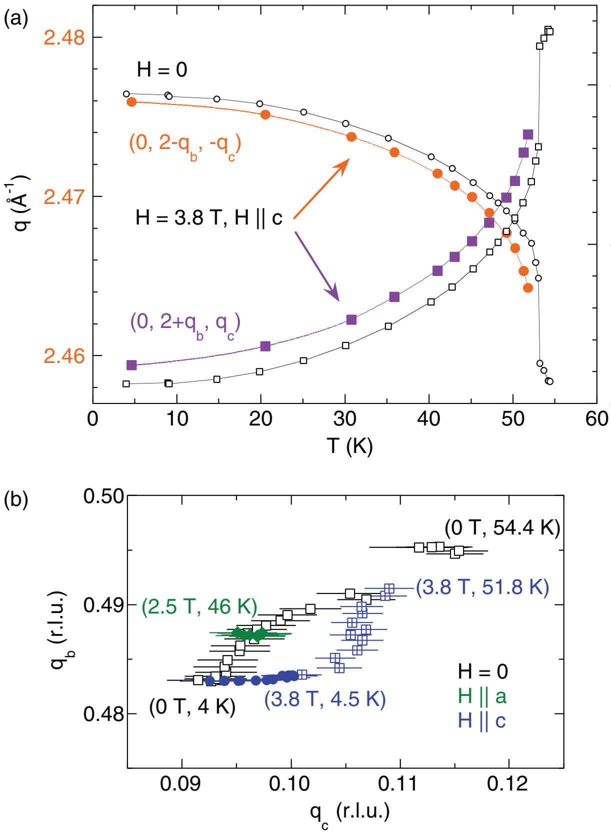

FIG. 9. (Color online) Evolution of the spin-ordering wave vector as a function of field and temperature. (a) Temperature dependence of magnetic orders $(0,\ 2\pm q_b,\ \pm q_c)$, for $H\|c$ at $T=4.5$ K compared to those at $H=0$ (Ref. 10). (b) Evolution of $(q_b,\ q_c)$ in the KL plane of reciprocal space for $H=0$ (black), $H\|c$ at $T=4.5$ K (solid blue) and from 4.5 to 51.8 K (open blue) and $H\|a$ at $T=46$ K (green).

The evolution of the spin ordering wave vector in KL space as a function of H and T in Fig. 9 indicates minimal changes in the magnetic portion of the Fermi surface with field. This conclusion is buttressed by the insensitivity to field of the shape and size of the temperature-dependent resistance anomaly up to at least $H=9$ T [Figs. 6(a), 6(b)]. The resistance anomaly at the onset of spin density wave ordering in GdSi indicates a gap opening on the Fermi surface as the nesting condition is satisfied.[10] The stability of q and the gap in field is also seen for the SDW in chromium, where the incommensurate antiferromagnetic order survives in a field of 16 Tesla[25] and the itinerant spin moments that are transverse to the ordering wave vector rotate with applied magnetic field while the magnetic wave vector remains constant,[26] and in the commensurate rare earth magnet Gd_5Ge_4, where spin directionality follows the applied field, while the antiferromagnetic wave vector stays constant.[18] We also note that the shape of $Q(T)$ in Fig. 9 is characteristic of SDW-type Fermi surface instabilities,[1,27] whereas for RKKY-driven incommensurate spin structures, such as $GdNi_2B_2C$, $Q(T)$ is not necessarily monotonic.[28]

The independence between the ordering wave vector and the spin orientation in the pure spin system GdSi can be compared with other spin ordering mechanisms such as the topologically nontrivial Skyrmion state,[29,30] notably in the related compound MnSi. In systems with both a noncentrosymmetric crystalline lattice and orbital moments, a spiral magnetic order can develop due to the Dzyaloshinsky-Moriya interaction between neighboring orbital moments. The spiral axis of the order is determined by the local interaction, and, as the magnetic moments realign under the influence of an applied field, the magnetic ordering wave vector changes.[29] Skyrmion systems do not necessarily have a long-range order beyond the size of one Skyrmion state.[30] By contrast, the spin order in GdSi involves the Fermi sea of electrons with a magnetic wave vector that arises from a global instability of mean-field character.[2] The magnetic wave vector is determined by electron counting, making it relatively insensitive to magnetic fields, and its energy scale is tiny in comparison to the Fermi energy. Experimentally, we observe a magnetic correlation length of at least 1500 Å in GdSi under all field and temperature conditions.

V. CONCLUSIONS

The incommensurate SDW state in GdSi displays an intricate H-T phase diagram, reflecting aspects of both the long-range nature of the Fermi electron sea and Gd local moment physics. The $\boldsymbol{Q}$ vector and SDW gap are relatively insensitive to applied magnetic field—dominated by the global characteristics of Fermi surface nesting—but the spin structures are highly pliable. Spins rotate relative to H through either canting or spin-flop processes, leading to antiferromagnetic spin densities that tend to arrange themselves transverse to the applied magnetic field. The resulting H-T phase diagrams are characterized by two types of phase lines: one separates a collinear ordering from a planar spin structure, in association with a lattice structural transition, and the other is determined by a spin-flop transition and is independent of temperature over a broad range in T. An essentially isotropic value of the magnetic field, $H = 20.7 \pm 0.1$ T, completely suppresses the antiferromagnetism at $T = 0$ along each of the three crystalline axes, consistent with the small single-ion anisotropy of the Gd spins.

ACKNOWLEDGMENTS

The work at the University of Chicago was supported by National Science Foundation Grant No. 1206519 and used MRSEC shared facilities, NSF Grant No. DMR-0820054. The work at the Advanced Photon Source of Argonne National Laboratory was supported by the U.S. Department of Energy Basic Energy Sciences under Contract No. NE-AC02-06CH11357. Work performed at the National High Magnetic Field Laboratory was supported by National Science Foundation Cooperative Agreement No. DMR-1157490, the State of Florida, and the U.S. Department of Energy. Work at Oak Ridge National Laboratory was supported by the Materials Sciences and Engineering Division, DOE-BES. A.P. was supported in part by DOE-SCGF under Contract DE-AC05-06OR23100.

---

[1] E. Fawcett, Rev. Mod. Phys. **60**, 209 (1988).

[2] A. W. Overhauser, Phys. Rev. **128**, 1437 (1962).

[3] J. M. Barandiaran, D. Gignoux, D. Schmitt, and J. C. Gomez Sal, Solid State Commun. **57**, 941 (1986).

[4] Z. Islam *et al.*, Phys. Rev. Lett. **83**, 2817 (1999).

[5] W. Good, J. Kim, A. I. Goldman, D. Wermeille, P. C. Canfield, C. Cunningham, Z. Islam, J. C. Lang, G. Srajer, and I. R. Fisher, Phys. Rev. B **71**, 224427 (2005).

[6] J. W. Lynn, S. Skanthakumar, Q. Huang, S. K. Sinha, Z. Hossain, L. C. Gupta, R. Nagarajan, and C. Godart, Phys. Rev. B **55**, 6584 (1997).

[7] H. Pinto, M. Melamud, M. Kuznietz, and H. Shaked, Phys. Rev. B **31**, 508 (1985).

[8] S. L. Bud'ko, Z. Islam, T. A. Wiener, I. R. Fisher, A. H. Lacerda, and P. C. Canfield, J. Magn. Magn. Mater. **205**, 53 (1999).

[9] B. D. Hennings, D. G. Naugle, and P. C. Canfield, Phys. Rev. B **66**, 214512 (2002).

[10] Y. Feng *et al.*, Proc. Nat. Acad. Sci. U.S.A. **110**, 3287 (2013).

[11] D. A. Nagaki and A. Simon, Acta Crystallogr. C **46**, 1197 (1990).

[12] H. Saito, S. Suzuki, K. Fukamichi, T. Mitamura, and T. Goto, J. Phys. Soc. Jpn. **65**, 1938 (1996).

[13] L. D. Tung, M. R. Lees, G. Balakrishnan, D. McK. Paul, P. Schobinger-Papamantellos, O. Tegus, P. E. Brommer, and K. H. J. Buschow, Phys. Rev. B **71**, 144410 (2005).

[14] R. Daou, F. Weickert, M. Nicklas, F. Steglich, A. Haase, and M. Doerr, Rev. Sci. Instrum. **81**, 033909 (2010).

[15] H. Li, Y. Xiao, B. Schmitz, J. Persson, W. Schmidt, P. Meuffels, G. Roth, and T. Bruckel, Sci. Reports **2**, 750 (2012).

[16] M. Blume and D. Gibbs, Phys. Rev. B **37**, 1779 (1988).

[17] From our measurements, we believe that the c axis and a axis magnetization curves in Fig. 2 of Ref. 13 have been mistakenly interchanged.

[18] L. Tan *et al.*, Phys. Rev. B **77**, 064425 (2008).

[19] S. Takayanagi, Y. Ōnuki, K. Ina, T. Komatsubara, N. Wada, T. Watanabe, T. Sakakibara, and T. Goto, J. Phys. Soc. Jpn. **58**, 1031 (1989).

[20] Y. Yamaguchi, K. Ohoyama, H. Yamauchi, K. Indoh, and H. Onodera, Appl. Phys. A **74**, s877 (2002).

[21] M. Rotter, M. Loewenhaupt, M. Doerr, A. Lindbaum, H. Sassik, K. Ziebeck, and B. Beuneu, Phys. Rev. B **68**, 144418 (2003).

[22] A. Castets, D. Gignoux, and J. C. Gomez-Sal, J. Solid State Chem. **31**, 197 (1980).

[23] J. A. Blanco, D. Gignoux, J. C. Gómez Sal, J. R. Carvajal, J. R. Fernández, and D. Schmitt, Physica B **180-181**, 100 (1992).

[24] J. A. Blanco, J. I. Espeso, J. García Soldevilla, J. C. Gómez Sal, M. R. Ibarra, C. Marquina, and H. E. Fischer, Phys. Rev. B **59**, 512 (1999).

[25] S. A. Werner, A. Arrott, and H. Kendrick, J. Appl. Phys. **37**, 1260 (1966).

[26] S. A. Werner, A. Arrott, and M. Atoji, J. Appl. Phys. **40**, 1447 (1969).

[27] E. E. Rodriguez, C. Stock, K. L. Krycka, C. F. Majkrzak, P. Zajdel, K. Kirshenbaum, N. P. Butch, S. R. Saha, J. Paglione, and M. A. Green, Phys. Rev. B **83**, 134438 (2011).

[28] C. Detlefs, A. I. Goldman, C. Stassis, P. C. Canfield, B. K. Cho, J. P. Hill, and D. Gibbs, Phys. Rev. B **53**, 6355 (1996).

[29] S. Mühlbauer, B. Binz, F. Jonietz, C. Pfleiderer, A. Rosch, A. Neubauer, R. Georgii, and P. Böni, Science **323**, 915 (2009).

[30] X. Z. Yu, Y. Onose, N. Kanazawa, J. H. Park, J. H. Han, Y. Matsui, N. Nagaosa, and Y. Tokura, Nature **465**, 901 (2010).

[31] P. S. Normile, M. Rotter, C. Detlefs, J. Jensen, P. C. Canfield, and J. A. Blanco, Phys. Rev. B **88**, 054413 (2013).